J. Fluid Mech. (1997), *vol.* 342, *pp.* 355–375. Printed in the United Kingdom

Opposing mixed convection flow in a wall jet over a horizontal plate

By F. J. HIGUERA

ETS Ingenieros Aeronáuticos, Pza. Cardenal Cisneros 3, 28040 Madrid, Spain

(Received 3 April 1996 and in revised form 10 September 1996)

The coupling of the temperature and velocity fields by buoyancy in a laminar two-dimensional wall jet over a finite-length horizontal plate is studied numerically and analytically in the asymptotic limit of infinite Reynolds number. Two configurations are considered leading to a cold layer of fluid over the plate, namely an ambient-temperature jet over a cooled plate and a cold jet over an insulated plate. In both cases buoyancy generates an adverse pressure gradient that may separate the flow if the Froude number is sufficiently small and always makes the solution everywhere over the plate dependent on the conditions at the downstream boundary. In the limit of very small Froude number separation occurs in a viscous–inviscid interaction region near the origin of the jet, leading to a separation bubble that covers a fraction of the plate dependent on the Prandtl number. The scalings of the solution in this asymptotic limit are obtained by order of magnitude estimations in the different regions of the bubble and in the buoyancy-dominated flow beyond the bubble, and the results are checked against the numerical solutions of the boundary layer equations. A separate analysis is carried out for very large Prandtl numbers showing that the recirculation bubble is then much shorter than the plate, also in agreement with the numerical results.

1. Introduction

The most characteristic feature of high-Rayleigh-number natural convection around horizontal surfaces is perhaps the indirect way in which buoyancy generates the flow, by means of a hydrostatic pressure distribution in the vertical direction whose horizontal gradient pushes the fluid along the surface. The pressure gradient, therefore, is not known in advance, contrarily to the case of a buoyancy-free boundary layer, but must be determined as part of the solution. The resulting mathematical problem for the boundary layer flow is not parabolic, because this feature introduces a mechanism of influence of the downstream conditions on the evolution of the boundary layer. The same is true in principle of mixed-convection flows. Then the buoyancy-induced pressure gradient can either aid or oppose the forced flow, and the relative importance of the momentum of the forced flow to the effect of the buoyancy, measured by a Froude number, typically changes along the boundary layer.

The mutual dependence of the pressure and the motion of the fluid is the hallmark of interacting boundary layers. Buoyancy-induced interaction occurs here over the whole boundary layer, a feature shared with hypersonic external flows but at variance with many other external flows, for which the interaction is often confined to small regions whose size tends to zero as the Reynolds number tends to infinity (Smith 1982).

Under appropriate conditions, however, buoyancy may also lead to localized events in regions of large local Froude number, in the form of free interactions whereby the solution rapidly departs from the smooth flow that would otherwise occupy such regions. This dual character was pointed out by Gajjar & Smith (1983) and Bowles & Smith (1992) for the related problem of a liquid layer flowing over a horizontal plate, for which the interaction region was found to be a two-tier structure containing a lower viscous sublayer of low-velocity flow, which is the only one affected by the gradient of the gravity-induced pressure variations, and an upper tier where these variations are built by displacing vertically the fluid an amount determined by the viscous sublayer. Bowles & Smith (1992) showed that the equations of motion in the interaction region have solutions with separation, which are the abrupt (in the scale of the overall flow) beginning of transitions properly termed hydraulic jumps, and advanced that the same phenomenon can occur in thermally stratified layers. The subsequent evolution of the separated flow was analysed by Higuera (1994), showing that the local Froude number changes from very large to very small values across the hydraulic jump, and the flow adjusts to the boundary conditions imposed at the downstream end of the layer, which also determine the position of the interaction region.

Upstream information propagation through the thermal layer has led to some uncertainty in the solution of these boundary layer problems, particularly for opposing flow configurations. Apart from some self-similar solutions for a uniform outer stream and special plate temperature distributions, or for an adiabatic plate, which exist when the Froude number is above a certain value and typically exhibit multiplicity (Schneider 1979; Daniels 1993), difficulties often appear when a marching numerical method is used, in the form of a singularity whose position, and even its character, seems to depend on the particular numerical method and other approximations used (Schneider, Steinrück & Andre 1994). Daniels (1992) proved the existence of a characteristic singularity, and Daniels & Gargaro (1993) found that this singularity is approached by the numerical solution of the boundary layer equations for a layer of initially cold fluid over an adiabatic plate if the Froude number is sufficiently small. Steinrück (1994) analysed the spectrum of the linearized boundary layer operator and discretizations thereof, showing that it is not uniformly bounded from above, which results in the collapse of any marching method at some distance from the origin of the boundary layer. It seems clear, therefore, that a different numerical method, not relying on streamwise marching and properly taking into account the downstream conditions, is called for.

In this paper, in order to study the effect of upstream information propagation in its simplest form, a planar wall jet flowing over a finite-length horizontal plate in the absence of any outer stream is considered, with an opposing pressure gradient generated by two alternative methods: either the jet issues at ambient temperature over a cooled plate or it issues at a temperature lower than the ambient over an adiabatic plate. Both flows are simple but realistic configurations of interest in heat transfer. The second one, in particular, is a model of the environment found near two of the corners of a thermally driven cavity. Only pressure variations due to the buoyancy are included in the analysis; additional pressure variations due to the curvature of the streamlines, which can be important in some cases and may lead to an interaction region of a different type (Smith & Duck 1977), are left out here. An additional advantage of the finite-length plate configuration, from the point of view of the analysis, is that it provides a clear specification of the boundary conditions at the end of the layer, where the cold fluid turns around the edge. These conditions were found by a local

analysis carried out elsewhere (Higuera 1993). As in many other configurations, the effect of the buoyancy is negligible here near the origin of the jet, and generates an adverse pressure gradient of increasing magnitude as the flow slows down and the thickness of the cold layer increases in the streamwise direction. Numerical solutions show that the flow first separates when an overall Froude number measuring the ratio of inertia to buoyancy in the scale of the plate falls below a certain value, and the region of reverse flow grows when this Froude number is further decreased. Special attention is paid to the limit of small overall Froude numbers. In this limit separation occurs near the origin of the jet in the Bowles–Smith interaction region mentioned before, the flow in the rest of the hydraulic jump is also similar to that of a separated liquid layer (Higuera 1994), and the flow farther downstream is dominated by the buoyancy-induced pressure gradient. This pressure gradient is now favourable, as the thickness of the cold layer decreases on approaching the end of the plate, and this seems in fact the main advantage derived by the flow from the early separation. The structure of the solution is somewhat different for very large Prandtl numbers. Then the thermal layer is confined to the base of the wall jet, where the effect of the inertia is negligible and the forced flow is felt through the shear stress that it impresses onto this layer. Here too separation occurs when the overall Froude number decreases, and the asymptotic solution for very small Froude numbers exhibits a short, single-tiered, separation region followed by a small recirculation bubble and a region of favourable pressure gradient that covers most of the plate.

The case of an ambient-temperature jet over a cold wall is analysed in §2, describing in turn the numerical solutions of the boundary layer problem, the asymptotic limit of large local Froude number, and the limits of large and small Prandtl numbers. The case of a cold jet over an insulated plate is more briefly analysed in §3, focusing on the differences with the previous case. The paper ends with a summary of the main results and a short discussion of their possible relevance to the problem of thermally driven cavities.

2. Ambient-temperature jet over a cold wall

2.1. *Formulation and numerical results*

Consider a plane wall jet flowing over a horizontal plate kept at a temperature ΔT below the ambient temperature T_∞ of the fluid above the jet. The apparent origin of the jet is at a distance l from the edge of the plate toward which is flow is directed. In the boundary layer approximation and in the absence of body forces the quantity $P = \int_0^\infty u \left(\int_y^\infty u^2 \, \mathrm{d}y_1 \right) \mathrm{d}y$, where u is the horizontal component of the flow velocity and the integrals are taken across the section of the jet, does not depend on the distance x to the apparent origin, and the flow in the jet becomes self-similar (Glauert 1956) downstream of a development region whose length depends on the injection conditions and will be neglected here. Under the action of gravity, the increase of density due to the cooling of the fluid near the plate leads to pressure variations in the jet whose gradient opposes the forced flow over part of the plate. Assuming that $\rho = \rho_\infty[1 - \beta(T - T_\infty)]$, where β is the thermal expansion coefficient of the fluid; using the factors l and $y_c = \nu^{3/4} l^{3/4} / P^{1/4}$ to scale the distances along the plate and normal to it, and $u_c = P^{1/2}/(\nu^{1/2} l^{1/2})$, $v_c = u_c y_c / l$ and $p_c = \rho_\infty g \beta \Delta T y_c$ for the corresponding components of the velocity and the pressure variation; and defining $\theta = (T_\infty - T)/\Delta T$, the boundary layer equations with the Boussinesq approximation

take the form

$$\nabla \cdot \boldsymbol{v} = 0\,, \tag{1}$$

$$\boldsymbol{v} \cdot \nabla u = -S\frac{\partial p}{\partial x} + \frac{\partial^2 u}{\partial y^2}\,, \tag{2}$$

$$\frac{\partial p}{\partial y} = -\theta\,, \tag{3}$$

$$\boldsymbol{v} \cdot \nabla \theta = \frac{1}{Pr}\frac{\partial^2 \theta}{\partial y^2}\,, \tag{4}$$

to be solved with the boundary conditions

$$y = 0 : u = v = \theta - 1 = 0\,, \tag{5}$$

$$y \to \infty : u = \theta = p = 0\,, \tag{6}$$

$$x \to 0 : \psi = x^{1/4} f(\eta), \quad \theta = g(\eta), \quad \eta = y/x^{3/4}\,, \tag{7}$$

$$x \to 1 : (1-x)^{\sigma}\partial p/\partial x < \infty, \quad \sigma \approx 0.6920\,. \tag{8}$$

Here Pr is the Prandtl number and

$$S = \frac{g\beta\Delta T \nu^{7/4} l^{7/4}}{P^{5/4}} \tag{9}$$

is the inverse of a Froude number, measuring the influence of the buoyancy-generated pressure force on the scale of the plate length. In (7) ψ is the stream function, with $u = \partial\psi/\partial y$, $v = -\partial\psi/\partial x$ and $\psi = 0$ at the plate, and the functions $f(\eta)$ and $g(\eta)$ are Glauert's self-similar solution, obtained solving the problem

$$\left.\begin{aligned} &f''' + \tfrac{1}{4} f' f'' + \tfrac{1}{2} f'^2 = 0, \qquad g'' + \tfrac{1}{4} Pr f g' = 0, \\ &f(0) = f'(0) = g(0) - 1 = 0, \quad f'(\infty) = g(\infty) = 0, \quad \int_0^\infty f' \left(\int_\eta^\infty f'^2 \, \mathrm{d}\eta_1 \right) \mathrm{d}\eta = 1\,. \end{aligned}\right\} \tag{10}$$

The boundary condition (8) at the edge of the plate comes from a local analysis carried out elsewhere (Higuera 1993), which shows that the buoyancy-induced pressure gradient is favourable and tends to infinity as $(1-x)^{-\sigma}$. Under the action of this force viscous effects are confined to a sublayer of thickness vanishing for $x \nearrow 1$, while the flow of the cold fluid in the rest of the boundary layer is effectively inviscid and approaches a limiting form at the edge which is independent of the evolution farther downstream. This last property is most convenient here, in order to set up a closed problem.

Equations (1)–(8) were numerically solved using a pseudo-transient finite difference method that circumvents the difficulties inherent to marching methods and allows for regions of reverse flow. This method essentially amounts to adding time derivatives to the left-hand sides of (2) and (4) and letting the flow evolve in time until a steady state is attained. The numerical results are commented on in the remainder of this section.

Of primary interest is the influence on Glauert's solution, corresponding to $S = 0$, of the gradient of the pressure variation due to the gravity. The pressure distribution across the jet, given by the hydrostatic balance (3) in the vertical direction, depends on the local thickness and temperature distribution of the cold fluid, being determined by the flow itself. The gradient of this pressure is adverse but has a negligible

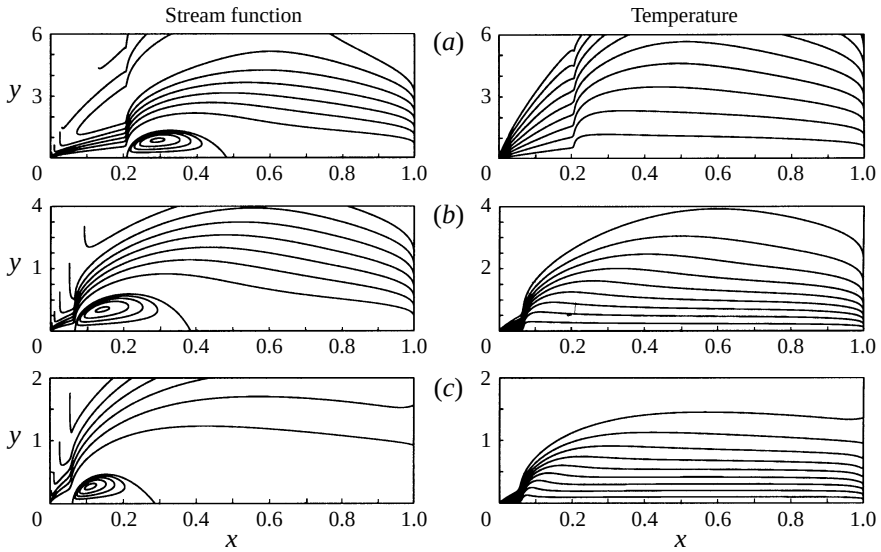

FIGURE 1. Streamlines and isotherms for: (*a*) $Pr = 0.1$, $S = 0.05$; (*b*) $Pr = 2$, $S = 0.4$; (*c*) $Pr = 20$, $S = 2.5$. Streamline spacing is 0.2 in the forward flow. In the bubble four equispaced streamlines are displayed in the three cases, the stream function on the innermost one being -0.025 in (*a*), -0.05 in (*b*), and -0.01 in (*c*). The spacing of the isotherms is 0.1. Notice the different vertical scales.

influence near the origin of the jet, where, using the self-similar solution (7) in (3) and (2), $(S\partial p/\partial x)/(\boldsymbol{v}\cdot\nabla u) = O(Sx^{7/4}) \ll 1$. On the other hand, the pressure gradient is favourable and dominates the flow near the edge of the plate for any $S > 0$. In between, the gradient remains adverse over the fore part of the plate and has a growing influence on the jet, which opens up faster than in Glauert's solution, reinforcing the adverse gradient, until the thickness of the cold layer reaches a maximum and begins to decrease under the influence of the edge of the plate. The deceleration of the flow becomes more pronounced when S increases, until separation of the wall jet, with the appearance of a recirculation bubble, occurs for a certain critical value of this parameter. The critical S is an increasing function of Pr, and the distance from the origin of the jet to the point where separation first occurs is a decreasing function of Pr. As S increases pass its critical value the bubble becomes larger, the separation point continuously approaches the origin, and the reattachment point also moves toward the origin, apparently tending to a limiting position whose distance to the origin is a decreasing function of Pr. The pressure gradient becomes favourable on the whole section of the jet shortly downstream of the reattachment point. An effect of separation is to reduce the loss of momentum of the jet by viscous friction with the wall and, by this means, the separated flow can negotiate the increasingly adverse pressure force.

Some streamlines and isotherms from representative computations are displayed in figure 1, and the distributions of skin friction and heat flux toward the plate are given in figure 2 for several values of S and Pr. As can be seen in figure 1, the shape of the streamlines in the upper part of the jet depends strongly on the Prandtl number. For sufficiently large values of this parameter the layer of cold fluid is confined to the fast moving jet, thickening only when the jet separates and becoming thin again farther downstream. The tendency of the cold layer to spread also toward the left is arrested by the push of the jet, and the fluid above the

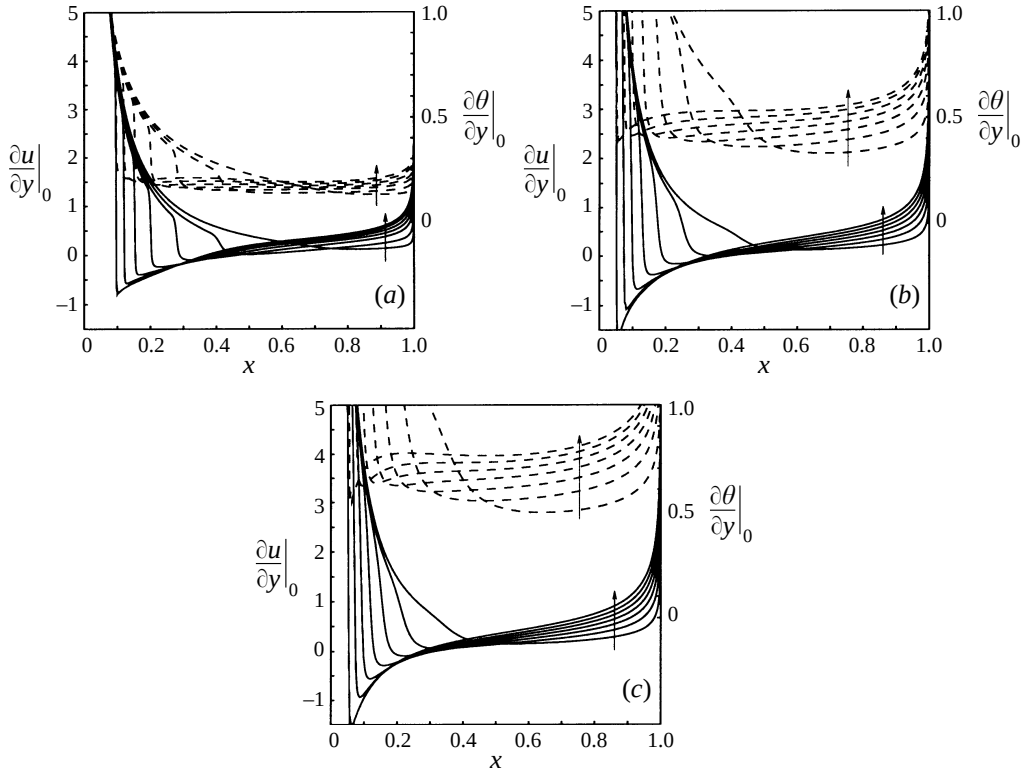

FIGURE 2. Skin friction (solid) and heat flux (dashed) for (*a*) $Pr = 0.5$ and $S = 0.02$, 0.04, 0.06, 0.08, 0.1, 0.12, 0.14; (*b*) $Pr = 3$ and $S = 0.1$, 0.2, 0.3, 0.4, 0.5, 0.6, 0.7; (*c*) $Pr = 7$ and $S = 0.2$, 0.4, 0.6, 0.8, 1, 1.2, 1.4. Values of S increasing as indicated by the arrows.

jet always moves toward the right. On the other hand, heat conduction leads to appreciable stratification above the jet for sufficiently small values of the Prandtl number, and the fluid in this region moves toward the left upstream of the separation point. The results displayed in figure 1 were obtained by solving the problem in terms of the variables x and $\eta = y/x^{3/4}$, which amount to having a computational domain of vanishing thickness for $x \to 0$. Further computations carried out with variables that allow a computational domain of non-zero thickness at the origin of the jet showed that the conditions at this section have an effect on the flow when the cold layer extends above the jet. If outflow is permitted at $x = 0$ (as when the plate does not extend to $x < 0$ or is kept at ambient temperature there), the thickness of the thermal layer decreases toward the origin, leading to a strong adverse pressure gradient on the jet. If no outflow is permitted, the adverse pressure gradient on the jet is weaker and decreases with Pr, and the flow over most of the plate begins to resemble the natural convection flow in the absence of the jet when S becomes large.

The skin friction for $x \to 0$ is of the form $\partial u/\partial y|_0 = \lambda/x^{5/4}$, with $\lambda \equiv f''(0) = (5/2)^{3/4}/9 \approx 0.2209$ from the solution of (10), whereas it is proportional to $(1 - x)^{-(3\sigma-1)/4}$ for $(1 - x) \ll 1$. The corresponding expressions of the heat flux are $\partial\theta/\partial y|_0 = \lambda_1/x^{3/4}$ and $(1 - x)^{-\kappa}$, where λ_1 and κ depend on the Prandtl number. For all but very small values of S both of these quantities branch off rather abruptly from their asymptotic forms for x small, at a point practically coinciding with the

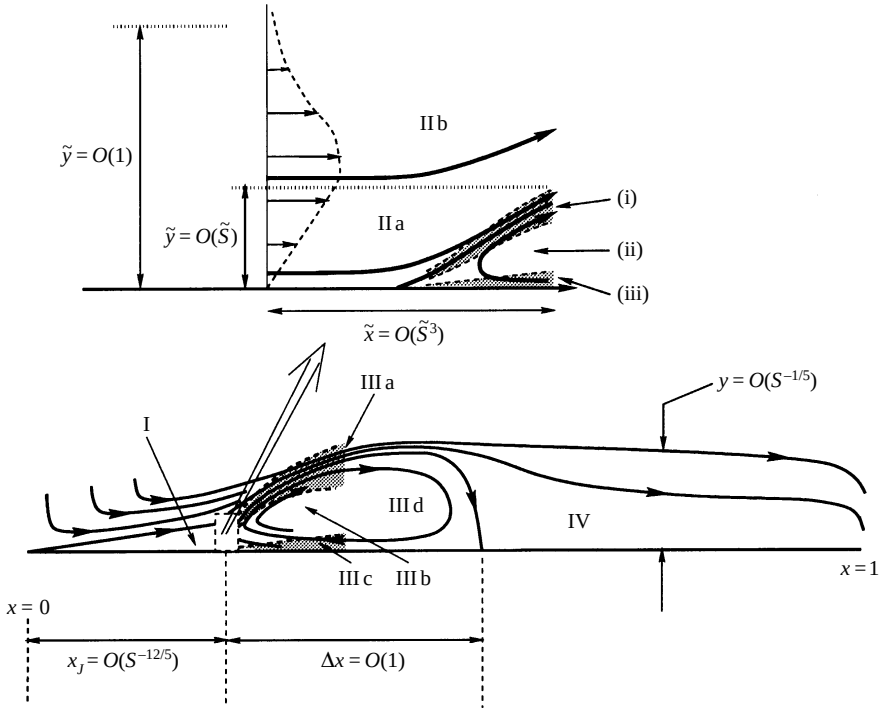

FIGURE 3. Sketch of the asymptotic solution for $S \to \infty$.

separation point of the wall jet when S is above its critical value. This feature is not clearly visible in figure 2 but the associated effect on the streamlines can be seen in figure 1. It will appear in the discussion that follows.

2.2. *Asymptotic limit* $S \to \infty$

The numerical results seem to support the view that a solution of the problem (1)–(8) exists for arbitrarily large values of S. The asymptotic structure of this solution for $S \to \infty$ will be analysed in this section. Many aspect of this structure are similar to that of a hydraulic jump in a horizontal liquid layer, studied by Bowles & Smith (1992) and Higuera (1994), and the following description relies heavily on these works.

Separation occurs at a distance $x_J \ll 1$ from the origin when $S \gg 1$, and the flow upstream of the separation point is little affected by the pressure gradient. In addition to the non-separated jet, two large regions can be distinguished in the flow, namely the recirculation bubble and the region of forward flow further downstream, and it turns out that an order of magnitude analysis of the flow in these regions suffices to determine the order of x_J and other important features of the asymptotic solution. The variables $\tilde{x} = x/x_J - 1$, $\tilde{y} = y/x_J^{3/4}$, $\tilde{u} = x_J^{1/2}u$, $\tilde{v} = x_J^{3/4}v$ and $\tilde{p} = p/x_J^{3/4}$ will be used to describe the flow around the separation point and in the bubble. Equations (1)–(4) conserve their form when rewritten in these variables, with S replaced by $\tilde{S} = Sx_J^{7/4}$, which can be made to be small to account for the abruptness of the separation and the near absence of pressure

effects in the non-separated jet. Figure 3 is a sketch of the different regions of the flow.

The process leading to separation of the jet with $\tilde{S} \ll 1$ occurs in the short viscous–inviscid interaction region II at the nose of the separation bubble (see upper part of figure 3). The universal structure of this region was first analysed by Gajjar & Smith (1983) and Bowles & Smith (1992), and their results can be summarized as follows. The interaction region extends over a length $\tilde{x} = O(\tilde{S}^3)$, consisting of a viscous sublayer of low velocity IIa, where $(\tilde{y}, \tilde{u}) = O(\tilde{S})$ and the flow is affected by the buoyancy-induced pressure gradient, and the bulk of the jet IIb, which is merely displaced outward by the presence of the sublayer. Equations (1) and (2) hold in the viscous sublayer, where, as will be seen below, the non-dimensional pressure variation is equal to the unknown displacement of the jet, $= -\tilde{S}A\left(\tilde{x}/\tilde{S}^3\right)$ say. These equations must be solved subject to the boundary conditions (5) and the matching conditions with the upper region: $\tilde{u}/\tilde{S} \to \lambda\left[\tilde{y}/\tilde{S} + A(\tilde{x}/\tilde{S}^3)\right]$ for $(\tilde{y}/\tilde{S}) \to \infty$, and with the oncoming unperturbed jet: $\tilde{u} = \lambda\tilde{y}$, $A = 0$ for $(\tilde{x}/\tilde{S}^3) \to -\infty$. The numerical solution of this problem was obtained by Bowles & Smith (1992), who showed that the flow separates from the wall under the action of the self-induced pressure and that the solution takes on an asymptotic form $\tilde{x}/\tilde{S}^3 \gg 1$ consisting of (i) a shear layer of thickness $O\left[\tilde{S}(\tilde{x}/\tilde{S}^3)^{1/3}\right]$ at the base of the separated jet, (ii) a recirculation region of thickness $\tilde{y}_b = O\left[\tilde{S}(\tilde{x}/\tilde{S}^3)^m\right]$, with $m = \frac{2}{3}(\sqrt{7}-2) \approx 0.431$, where the flow is rotational and effectively inviscid, and (iii) a viscous sublayer at the base of the recirculation region. This sublayer is required to satisfy the non-slip condition at the wall and is the only region affected by the gradient of the self-induced pressure, which is of order $\tilde{y}_b/\tilde{x}$.

The temperature distribution in the interaction region is

$$\theta = \theta_0(\tilde{y} + \tilde{S}A) + \Delta\theta(\tilde{x}/\tilde{S}^3, \tilde{y}), \tag{11}$$

where $\theta_0(\tilde{y})$ is the temperature profile immediately upstream of the interaction region, extended as $\theta_0 = 1$ for $\tilde{y} < 0$. Here the shift $\tilde{S}A$ takes care of the displacement of the bulk of the jet and $\Delta\theta$ is of $O(\tilde{S})$ in the viscous sublayer IIa, where heat conduction matters, and much smaller, of $O(\tilde{S}^3)$, in IIb. Putting (11) into (3) yields $\tilde{p} = \int_{\tilde{y}}^{\infty} \theta \, \mathrm{d}\tilde{y} \approx \tilde{p}_0(\tilde{y}) - \tilde{S}A\theta_0(\tilde{y}) + \int_{\tilde{y}}^{\infty} \Delta\theta \, \mathrm{d}\tilde{y}$, where $\tilde{p}_0(\tilde{y}) = \int_{\tilde{y}}^{\infty} \theta_0(\tilde{y}) \, \mathrm{d}\tilde{y}$. Thus $\tilde{p} - \tilde{p}_0 = -\tilde{S}A$ to leading order in the viscous sublayer, as was advanced before.

The three regions (i) to (iii) mentioned above are continued downstream of the interaction region in the structure IIIa–IIIc, which is similar to that of a laminar hydraulic jump (Higuera 1994). The shear layer covers the whole of the separated jet when $\tilde{x} = O(1)$ and, since the influence of the pressure gradient on this flow is still negligible when $\tilde{S} \ll 1$, the jet IIIa takes on Bickley's self-similar form for $\tilde{x} \gg 1$: $\tilde{\psi} = 6\gamma\tilde{x}^{1/3} \tanh\left[\gamma(\tilde{y} - \tilde{y}_b(\tilde{x}))/\tilde{x}^{2/3}\right]$, with $\gamma = (\tilde{\phi}/48)^{1/3} \approx 0.2640$, where $\tilde{\phi} = 5^{3/4}2^{5/4}/9$ is the momentum flux of the wall jet at separation. Here $\tilde{y}_b = O(\tilde{x}^n/\tilde{S}^{(2-3n)/4})$, with $n = \frac{1}{6}(\sqrt{73} - 7) \approx 0.2573$, is the thickness of the recirculation region IIIb, determined by matching with the jet above and with the viscous sublayer IIIc at its bottom, which, as before, is affected by the pressure gradient. The pressure force, $O(\tilde{S}\tilde{y}_b/\tilde{x})$, due mainly to the cold fluid in the recirculation region, becomes of the order of the convective term in the momentum equation for the jet, $\boldsymbol{v} \cdot \nabla\tilde{u} = O(\tilde{x}^{-5/3})$, when $\tilde{x} = O(\tilde{S}^{-3/4})$, at which point the thickness of the jet is of the same order, $\tilde{S}^{-1/2}$, as the depth of the recirculation region and $\tilde{u} = O(\tilde{S}^{1/4})$. These scales correspond to the bulk of the recirculation bubble IIId, where the fluid turns around under the action of both the pressure

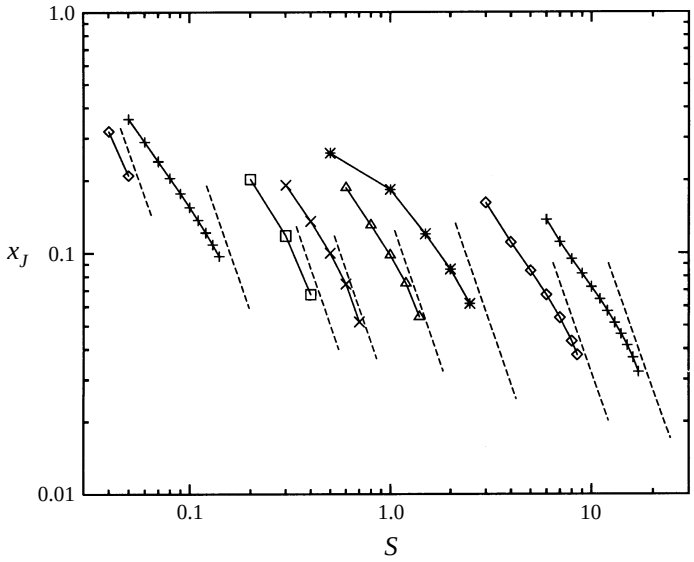

FIGURE 4. Position of the separation point as a function of S for $Pr = 0.1$, 0.5, 2, 3, 7, 20, 50 and 100, from left to right. The dashed lines have slope $-12/5$.

and the viscous forces as it cannot proceed much farther under an adverse pressure gradient.

The thickness of the cold layer decreases toward the edge of the plate in region IV, downstream of the reattachment section, leading to a favourable pressure gradient. The balance of inertia, pressure and viscosity in the momentum equation for $x = O(1)$ (i.e. $u^2 \sim Sy \sim u/y^2$) yields $y = O(S^{-1/5})$ and $u = O(S^{2/5})$ in this region, which are the scales of the natural convection flow originated by the cold plate in the absence of the jet. Finally, consistency with the previous results in the region of the bubble implies $x_J^{3/4}\tilde{y}_b \sim S^{-1/5}$, which is satisfied for $x_J = O(S^{-12/5})$, where also $x_J^{-1/2}\tilde{u} \sim S^{2/5}$. Carrying this estimation into the definition of $\tilde{S}$ gives $\tilde{S} = O(S^{-16/5})$, which is very much smaller than unity, as was advanced before, whereas the length of the bubble is of order $x_J\tilde{S}^{-3/4} = O(1)$. Thus, as could perhaps have been guessed from the outset, the wall jet separates sufficiently early to conserve enough momentum to go through the region of adverse pressure gradient (actually arresting the leftward-bound natural convection flow in this region if the Prandtl number is not small) and reattaches only when the pressure gradient is about to become favourable, after a sizeable fraction of the plate length.

Figure 4 is a logarithmic representation of the position of the separation point, obtained from the numerical solutions, as a function of S for several values of Pr. As can be seen, the results approach straight lines of slope $-12/5$ even for moderate values of S.

2.3. *Solution for large Prandtl numbers*

In this limit the thickness of the thermal layer is of order $Pr^{-1/3}$ relative to the thickness of the wall jet, and the absence of recirculating flow above the jet seems guaranteed. Rescaling the vertical distance, horizontal velocity and pressure with $Pr^{-1/3}$, and defining $S_\infty = S/Pr^{2/3}$, the factor Pr dividing the conduction term in (4) moves to the left-hand side of the momentum equation (2). Taking then the limit

$Pr \to \infty$ one is left with the following problem in the thermal layer:

$$\nabla \cdot \boldsymbol{v} = 0, \tag{12}$$

$$-S_\infty \frac{\partial p}{\partial x} + \frac{\partial^2 u}{\partial y^2} = 0, \tag{13}$$

$$\frac{\partial p}{\partial y} = -\theta, \tag{14}$$

$$\boldsymbol{v} \cdot \nabla \theta = \frac{\partial^2 \theta}{\partial y^2}, \tag{15}$$

$$y = 0 : u = v = \theta - 1 = 0, \tag{16}$$

$$y \to \infty : \frac{\partial u}{\partial y} = \frac{\lambda}{x^{5/4}}, \quad \theta = p = 0, \tag{17}$$

$$x \to 0 : u = \frac{\lambda \eta}{x^{1/2}}, \quad \theta = g_\infty(\eta), \tag{18}$$

$$x \to 1 : (1-x)^{1/4} u < \infty \quad \text{for} \quad y/(1-x)^{1/4} \text{ finite}, \tag{19}$$

where the scaled variables are denoted with the same symbols as the original ones. Equation (17) is the matching condition of the thermal layer with the bulk of the jet above, stating that the latter region influences the flow in the thermal layer through the shear at the base of the jet. The self-similar temperature distribution of the wall jet near the origin is $g_\infty(\eta) = I(\eta)/I(0)$, with $I(\eta) = \int_\eta^\infty \exp\left(-\lambda \eta^3/24\right) \mathrm{d}\eta$ obtained from the second equation (10) with $f = \lambda \eta^2/2$. The boundary condition (19) is the analogue of (8) for an inertialess fluid. It comes from the balance of pressure and viscosity forces near the edge of the plate, where the diverging pressure gradient leads now to diverging velocities in the layer of cold fluid and renders heat conduction negligible. Thus, calling y_c the characteristic thickness of this layer at a distance $(1-x) \ll 1$ from the edge, (13) and (14) yield the order of magnitude relations $p/(1-x) \sim u/y_c^2$ and $p \sim y_c$, while the condition that the flux of cold fluid remains finite implies $u y_c \sim 1$, leading to the scales $(1-x)^{\pm 1/4}$ for the thickness and velocity. See Higuera (1993) for further details.

Numerical solution of the problem (12)–(19) shows that separation and a recirculation bubble first appear for S_∞ about 5. The skin friction and the heat flux in the region of the bubble are given in figure 5 for several values of S_∞, and the following trends are observed when this parameter increases: the height of the bubble increases; the separation point approaches the origin; the length of the bubble reaches a maximum and then decreases; and the reattachment point approaches the origin at about the same pace as the separation point.

A systematic account of these results can be obtained from the asymptotic solution of (12)–(19) for $S_\infty \to \infty$. As in the case of the previous subsection, the flow for $S_\infty \gg 1$ undergoes rapid changes in a short region around the separation point $x = x_J \ll 1$ where the pressure gradient first affects the motion. Here, following the same scheme as before, the flow in this region is analysed first and then the solutions in the recirculation region and beyond are discussed in turn, in order to find the compatibility conditions that determine the scale of x_J. Figure 6 is a sketch of the separation region. Introducing local (tilde) variables as in §2.2, equations (12)–(15) remain unaltered if S_∞ is changed to $\tilde{S}_\infty = S_\infty x_J^{7/4}$, which must be small for consistency. Now, in the absence of inertia, the balance of pressure and viscous

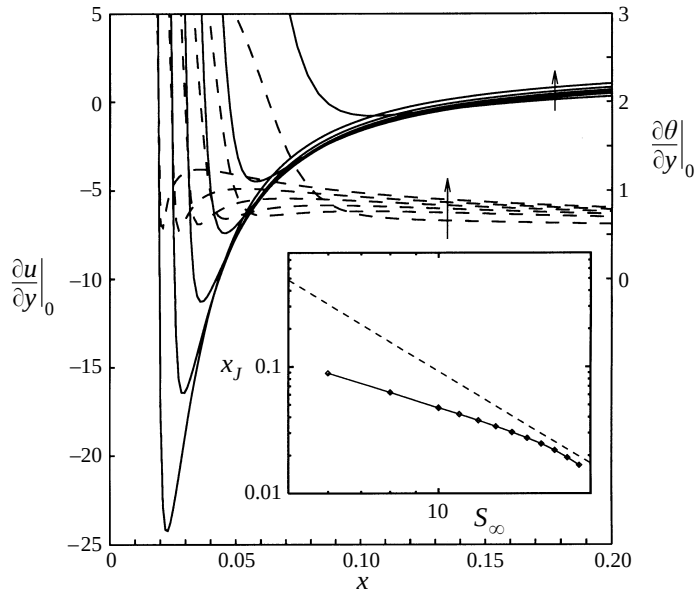

FIGURE 5. Skin friction (solid) and heat flux (dashed) for $Pr \to \infty$ and $S_\infty = 6$, 10, 12, 14, 16 and 18, increasing as indicated by the arrows. Inset: separation point as a function of S_∞. The dashed line has slope $-12/5$.

forces, with scaled velocities and pressures of order unity throughout the thermal layer (from (14) and the conditions of matching with the oncoming flow), precludes the existence of further sublayers and implies $\tilde{x} = O(\tilde{S}_\infty)$ in this region. Introducing then the variables $\bar{x} = \tilde{x}/\tilde{S}_\infty$ and $\bar{v} = \tilde{S}_\infty \tilde{v}$, we are led to the problem

$$\nabla \cdot \boldsymbol{v} = 0, \tag{20}$$

$$-\frac{\partial \tilde{p}}{\partial \bar{x}} + \frac{\partial^2 \tilde{u}}{\partial \tilde{y}^2} = 0, \tag{21}$$

$$\frac{\partial \tilde{p}}{\partial \tilde{y}} = -\theta, \tag{22}$$

$$\boldsymbol{v} \cdot \nabla \theta = 0, \tag{23}$$

$$\tilde{y} = 0 : \tilde{u} = \bar{v} = 0, \tag{24}$$

$$\tilde{y} \to \infty : \frac{\partial \tilde{u}}{\partial \tilde{y}} = \lambda, \quad \tilde{p} = 0, \tag{25}$$

$$\bar{x} \to -\infty : u = \lambda \tilde{y}, \quad \theta = g_\infty(\tilde{y}), \quad \tilde{p} = \int_{\tilde{y}}^{\infty} g_\infty \, \mathrm{d}\tilde{y}, \tag{26}$$

plus appropriate conditions for $\bar{x} \to \infty$ (see below), including $\theta = 1$ in the recirculating fluid.

Equations (20)–(23) can be rewritten as a single equation for the stream function. After a Prandtl transformation ($\tilde{Y} = \tilde{y} - \tilde{y}_b$, where $\tilde{y}_b(\bar{x})$ is the depth of the recirculation region, equal to zero for $\bar{x} < 0$), this equation becomes

$$\frac{\mathrm{d}\theta_0}{\mathrm{d}\tilde{\psi}} \left(\frac{\partial \tilde{\psi}}{\partial \bar{x}} - \tilde{y}_b' \frac{\partial \tilde{\psi}}{\partial \tilde{Y}} \right) + \frac{\partial^4 \tilde{\psi}}{\partial \tilde{Y}^4} = 0, \tag{27}$$

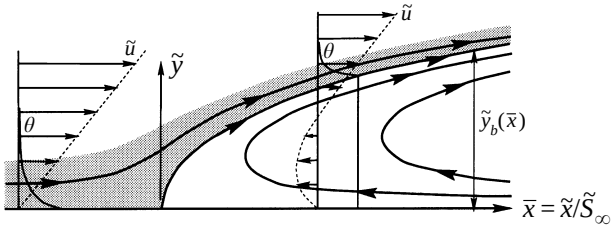

FIGURE 6. Sketch of the flow around the separation point for $S_\infty \to \infty$.

where $\theta_0(\tilde{\psi})(= g_\infty\left((2\tilde{\psi}/\lambda)^{1/2}\right)$ for $\tilde{\psi} > 0$ and $= 1$ for $\tilde{\psi} < 0$) is the temperature, which is conserved along the streamlines. In the recirculating flow ($\tilde{Y} < 0$) equation (27) reduces to $\partial^4\tilde{\psi}/\partial\tilde{Y}^4 = 0$, whose solution, with the conditions $\tilde{\psi} = \partial\tilde{\psi}/\partial\tilde{Y} = 0$ at $\tilde{Y} = -\tilde{y}_b$ and $\tilde{\psi} = 0$ at $\tilde{Y} = 0$, is $\tilde{\psi} = (\partial^3\tilde{\psi}/\partial\tilde{Y}^3)_{\tilde{Y}=0}\tilde{Y}(\tilde{Y}+\tilde{y}_b)^2/6$. In the forward flow ($\tilde{Y} > 0$) equation (27) must be solved for $\tilde{\psi}(\bar{x}, \tilde{Y})$ and $\tilde{y}_b$ subject to the conditions

$$\left.\begin{aligned} &\tilde{Y} = 0: \quad \tilde{\psi} = 0, \quad 4\frac{\partial\tilde{\psi}}{\partial\tilde{Y}} = \tilde{y}_b\frac{\partial^2\tilde{\psi}}{\partial\tilde{Y}^2}, \quad \frac{\partial\tilde{\psi}}{\partial\tilde{Y}} = \frac{\tilde{y}_b^2}{6}\frac{\partial^3\tilde{\psi}}{\partial\tilde{Y}^3}, \\ &\tilde{Y} \to \infty: \quad \frac{\partial^2\tilde{\psi}}{\partial\tilde{Y}^2} = \lambda, \quad \frac{\partial^3\tilde{\psi}}{\partial\tilde{Y}^3} = 0, \end{aligned}\right\} \tag{28}$$

where the last two conditions at $\tilde{Y} = 0$ express the continuity of the velocity and shear stress across the dividing streamline. Since $\mathrm{d}\theta_0/\mathrm{d}\tilde{\psi} \leqslant 0$, equation (27) is parabolic and its solution can be obtained marching in the $(-\bar{x})$ direction from a given state far downstream. The appropriate initial conditions for $\bar{x} \to \infty$ can be determined noticing that the layer of forward moving cold fluid on top of the recirculation bubble (the shaded region in figure 6) becomes much thinner than the bubble itself, and therefore the variations of pressure and shear stress across this layer can be neglected in a first approximation. Then the vertical hydrostatic balance (22) and the momentum equation (21) give $\tilde{p} = (\tilde{y}_b - \tilde{y})$ and $\tilde{u} = \tilde{y}_b'\tilde{y}(3\tilde{y} - 2\tilde{y}_b)/6$ (which is approximately equal to $\tilde{u}_0 = \tilde{y}_b'\tilde{y}_b^2/6$ throughout the layer of cold fluid), whereas the first condition (25) implies $\partial\tilde{u}/\partial\tilde{y}|_{\tilde{y}_b} = \lambda$; i.e. $2\tilde{y}_b\tilde{y}_b'/3 = \lambda$, or $\tilde{y}_b = (3\lambda\bar{x})^{1/2}$ asymptotically. The thickness of the layer of cold fluid is $O(\tilde{y}_b^{-1})$ (because $\tilde{u}_0 = O(\tilde{y}_b)$), and $\tilde{\psi} = \tilde{u}_0\tilde{Y}$ to leading order in this layer. Higher-order corrections can be easily worked out, leading to the required initial conditions for (27) (up to a shift of the origin):

$$\bar{x} \to \infty: \tilde{\psi} = \frac{\lambda\tilde{Y}^2}{2} + \left(\tilde{u}_0 - \frac{3}{\tilde{y}_b}\right)\tilde{Y} - \tilde{y}_b' G(\tilde{Y}) + o(\bar{x}^{-2}), \quad \tilde{y}_b = (3\lambda\bar{x})^{1/2} - \frac{2\sqrt{3}}{\lambda^{3/2}\bar{x}^{1/2}} + o(\bar{x}^{-1/2}), \tag{29}$$

where $G(\tilde{Y}) = \int_0^{\tilde{Y}}\int_0^{\tilde{Y}_1}\int_{\tilde{Y}_2}^{\infty}\theta_0(\tilde{u}_0\tilde{Y}_3)\,\mathrm{d}\tilde{Y}_3\,\mathrm{d}\tilde{Y}_2\,\mathrm{d}\tilde{Y}_1 = O(\bar{x}^{-3/2})$. The depth of the bubble and the skin friction obtained from the solution of (27)–(29) are given in figure 7 (solid curves). The decay of the solution toward the upstream state (26) for $\bar{x} \to -\infty$ can be analysed looking for small perturbations about this state, of the form $\tilde{\psi} = \lambda\tilde{Y}^2/2 + \mathrm{e}^{\mu\bar{x}}\tilde{\psi}'(\tilde{Y})$. Upon linearization of (27), the eigenvalue problem

$$\frac{\mathrm{d}^4\tilde{\psi}'}{\mathrm{d}\tilde{Y}^4} - \frac{\mu}{\lambda I(0)}\frac{\mathrm{e}^{-\lambda\tilde{Y}^3/24}}{\tilde{Y}}\tilde{\psi}' = 0,$$

$$\tilde{\psi}'(0) = \frac{\mathrm{d}\tilde{\psi}'}{\mathrm{d}\tilde{Y}}(0) = \frac{\mathrm{d}^2\tilde{\psi}'}{\mathrm{d}\tilde{Y}^2}(\infty) = \frac{\mathrm{d}^3\tilde{\psi}'}{\mathrm{d}\tilde{Y}^3}(\infty) = 0$$

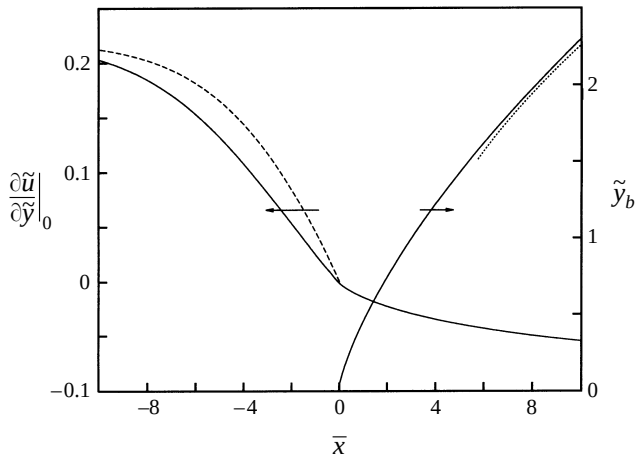

FIGURE 7. Skin friction and depth of the bubble in the region around the separation point for $Pr \to \infty$. Dashed: skin friction in the corresponding region for the flow of §3. Dotted: asymptotic expression (29).

is obtained, whose eigenvalues are all real and positive, the smallest one being $\mu_1 \approx 0.10$.

The balance of adverse pressure force and outer shear that led to (29) persists downstream of the separation region, except that the first condition (17) then becomes $\partial\tilde{u}/\partial\tilde{y}|_{\tilde{y}_b} = \lambda/(1+\tilde{x})^{5/4}$, instead of the simpler form in (25). The resulting $\tilde{y}_b(\tilde{x})$ would level off to a value of order $\tilde{S}_\infty^{-1/2}$ when $\tilde{x} \to \infty$, and the recirculating fluid slows down until the effect of the heat conduction finally affects the flow in the bulk of the bubble. A feature complicating this description of the flow and preventing a closed-form analytic solution being obtained is that the temperature is not uniform in the bulk of the bubble, and thus the pressure gradient can be adverse in some parts of a given section (most likely near the wall, judging by the appearance of the numerical solutions) and favourable in others. This, however, does not alter the foregoing estimate that the maximum depth of the bubble is of order $\tilde{S}_\infty^{-1/2}$ in tilde variables.

Beyond the bubble, and coming back to the original variables, the pressure–viscosity balance in the momentum equation (13) and the convection–conduction balance in the energy equation (15) yield $y = O(S_\infty^{-1/5})$ and $u = O(S_\infty^{2/5})$ in the thermal layer, much as in the previous Subsection. Equating this estimation of the thickness of the thermal layer to the order of the maximum depth of the bubble, $x_J^{3/4}\tilde{S}_\infty^{-1/2}$, gives $x_J = O(S_\infty^{-12/5})$ (whence $\tilde{S}_\infty = O(S_\infty^{-16/5}) \ll 1$), a result confirmed by the data in the inset of figure 5.

2.4. *Solution for small Prandtl numbers*

In the limit of very small Prandtl numbers the natural convection flow induced by the cooling of the plate would occupy a layer of thickness $\delta_n = O(S^{-1/5}Pr^{-2/5})$ where an effectively inviscid fluid would move with velocity $u_n = O(S^{2/5}/Pr^{1/5})$. The vertical velocity of this fluid would be $v_n = O(S^{1/5}/Pr^{3/5})$ and the pressure force pushing it $S\partial p/\partial x = O(S^{4/5}/Pr^{2/5})$. The presence of the wall jet impedes the development of this natural convection flow if $S \ll Pr^3$, because the ingestion of the

jet induces vertical velocities of $O(1) \gg v_n$ that suck in the cold fluid. If $S = O(Pr^3)$ the entrainment of the jet influences the much thicker thermal layer through the condition $v = -f(\infty)/(4x^{3/4})$, with $f(\infty) = 40^{1/4}$, effectively at $y = 0$. Numerical solution of the corresponding problem confirms that this influence becomes weak and confined to a small region near the origin of the jet when S/Pr^3 becomes large. On the other hand, it is not until $S = O(Pr^{1/2})$ that the velocity and pressure force in the thermal layer become of order unity and the presence of this layer begins to affect the jet, which, by then, has no influence on the thermal layer.

Focusing then on the limit $S_0 \equiv S/Pr^{1/2} = O(1)$ for $Pr \to 0$, it may be noticed that the effect of the thermal layer on the jet depends on the boundary conditions above the jet's origin. If no outflow of the thermal layer is possible there (for example if the wall jet is originated by a vertical free jet impinging on the plate) its thickness will decrease monotonically toward the edge of the plate, leading to a favourable pressure gradient everywhere on the jet. On the other hand, if outflow is possible at the left-side boundary, the thickness of the thermal layer will be maximum at some intermediate point between the origin of the jet and the edge of the plate, and the pressure gradient on the jet will be adverse between the origin and this point, leading to separation if S_0 is sufficiently large.

Provided that a solution exhibiting flow separation exists for $S_0 \gg 1$, its main features would be as follows. Separation of the wall jet must occur at $x_J \ll 1$ in order for the jet to conserve enough momentum to overcome the region of adverse pressure gradient. In addition, since the length of this region is of the order of the length of the plate, independently in fact of how large S_0 may be, so must be the length of the recirculation bubble. The velocity of the separated jet decays as $x_J^{-1/2}\left(x/x_J\right)^{-1/3}$ for $\tilde{x} = (x/x_J - 1) \gg 1$ (cf. §2.2), becoming of order $x_J^{-1/6}$ for $x = O(1)$, and the thickness of the jet is then of order $x_J^{1/12}$. Finally, consistency with the flow downstream of the bubble requires that this velocity be of the order of the natural convection velocity u_n estimated before or, equivalently, that the dynamic pressure in the jet be of the order of the natural-convection pressure variation. This condition gives $x_J = O(S_0^{-12/5})$, while the thickness of the reattached viscous layer at the base of the thermal boundary layer is of order $S_0^{-1/5}$.

The similarities and differences between the present case and the one described in §2.2 are discussed in the remainder of this Section.

The temperature profile in the interaction region around the separation point is much thicker than the wall jet, but this fact and the reverse flow above the jet do not alter the dominant balance in the viscous sublayer. In fact, putting the previous estimation of x_J into the scalings of Bowles & Smith (1992) summarized in §2.2, the length of the interaction region is seen to be of order S_0^{-12}, the thickness of the viscous sublayer and the velocity of the fluid in it are of orders S_0^{-5} and S_0^{-2}, respectively, and the pressure force due to the displacement of the viscous sublayer is $S\partial p/\partial x = O(S_0^8)$ locally, much larger than the pressure force due to the natural convection flow, of order $S_0^{4/5}$.

The results of §2.2 hold also downstream of the interaction region for sufficiently small values of x, with $\tilde{S}_0 = S_0 x_J^{7/4}$ taking the place of $\tilde{S}$. In particular, the self-induced pressure force is

$$S\frac{\partial p}{\partial x} = O\left(\frac{S_0^{12m-5}(x - x_J)^{m-1}}{Pr^{(3m-1)/2}}\right)$$

for very small values of $(x/x_J - 1)$, and

$$S\frac{\partial p}{\partial x} = O\left(S_0^{4/5} Pr^{(2+3n)/8} x^{n-1}\right)$$

for $x/x_J \gg 1$. This force becomes of order $S_0^{4/5}$ for $x - x_J$ of order $x_* = S_0^{\frac{12}{5}\frac{5m-2}{1-m}} Pr^{\frac{2-3m}{2(1-m)}}$ (if $x_* \ll x_J$, corresponding to $S_0 \ll Pr^{-\frac{5}{24}\frac{2-3m}{4m-1}}$) or $x_* = Pr^{\frac{2+3n}{8(1-n)}}$ (if $x_* \gg x_J$, corresponding to $S_0 \gg Pr^{-\frac{5}{96}\frac{2+3n}{1-n}}$), and the pressure force due to the natural convection flow on top of the jet takes over farther downstream, changing the growth rate of the bubble.

The solution in the bubble for $x = O(x_*)$ and beyond is slightly different from the one described in §2.2. The differences are summarized here for the case $x_* \gg x_J$; the alternative case $x_* \ll x_J$ is probably of less interest, requiring too small values of the Prandtl number. For $x = O(x_*)$ the separated jet is still not affected by the pressure force and keeps growing in the self-similar fashion of §2.2, transporting a mass flux proportional to $\phi_m = x_J^{1/4}(x/x_J)^{1/3} = O(S_0^{1/5} x^{1/3})$ that comes partially from the recirculation region. The depth of the recirculation region is $y_b = \alpha_0 x^{n_0}$, where α_0 and n_0 can be determined from the following considerations, analogous to those of §2.2. (I) The bulk of the recirculating flow is also not affected by the pressure force, moving with a velocity of order $\phi_m/y_b = O(S_0^{1/5} x^{1/3-n_0}/\alpha_0)$ to fulfil the entrainment of the jet. This velocity is conserved on each streamline, which are essentially horizontal, resulting in a velocity profile proportional to $S_0^{1/5} y^{1/3n_0-1}/\alpha_0^{1/3n_0}$. (II) Viscous and pressure forces are important in a viscous sublayer, of thickness y_v say, at the bottom of the recirculating flow. The velocity in the sublayer must be of order $u_v = S_0^{1/5} y_v^{1/3n_0-1}/\alpha_0^{1/3n_0}$ for consistency with the velocity distribution in the bubble. The balance of convection, pressure and viscosity $(u_v^2/x \sim S_0^{4/5} \sim u_v/y_v^2)$ then requires $\alpha_0 = O(S_0^{-1/5})$, $n_0 = 1/9$ and $y_v = O(x^{1/4}/S_0^{1/5})$. Notice that the viscous sublayer merges with the jet when $x = O(1)$.

3. Cold jet over an insulated plate

This configuration shares many features with the previous one. Only the differences will be discussed here, which are due to the existence of a limited defect of heat flux, supplied by the jet and distributed in various ways depending on the structure of the flow. The negative of the heat flux in the jet is $\phi_T = \int_0^\infty (T_\infty - T)\,\mathrm{d}y$, which permits defining a convenient scale for the temperature defect: $\Delta T = \phi_T/(u_c y_c) = \phi_T/(\nu l P)^{1/4}$, where u_c and y_c are the horizontal velocity and vertical distance scales introduced in §2. The temperature defect in the jet is of order ΔT if the influence of gravity is not dominant and the Prandtl number is of order unity. Using this ΔT in the definitions of p_c, θ and S, the boundary layer problem takes again the form (1)–(8) except for the obvious changes $\partial\theta/\partial y = 0$ at $y = 0$ and $\theta = g_1(\eta)/x^{1/4}$ for $x \to 0$, with $g_1(\eta) = cJ(\eta)$, $J(\eta) = \exp\left[-\frac{1}{4}Pr\int_0^\eta f\,\mathrm{d}\eta\right]$ and $c = \left(\int_0^\infty f' J\,\mathrm{d}\eta\right)^{-1}$. In addition, the condition $\int_0^\infty u\theta\,\mathrm{d}y = 1$ must be verified for any x.

Numerical solutions of this problem were computed as before. The appearance of the flow and its dependence on the parameters S and Pr are similar to those of §2. The skin friction and temperature of the wall are given in figure 8.

In the asymptotic limit $S \to \infty$ separation occurs at $x_J \ll 1$. The balance of inertia, pressure gradient and viscosity in the region of favourable pressure gradient downstream of the recirculation bubble $(u^2 \sim S\theta y \sim u/y^2)$ together with the energy conservation condition $u\theta y = O(1)$, which replaces the condition $\theta = O(1)$ used in the

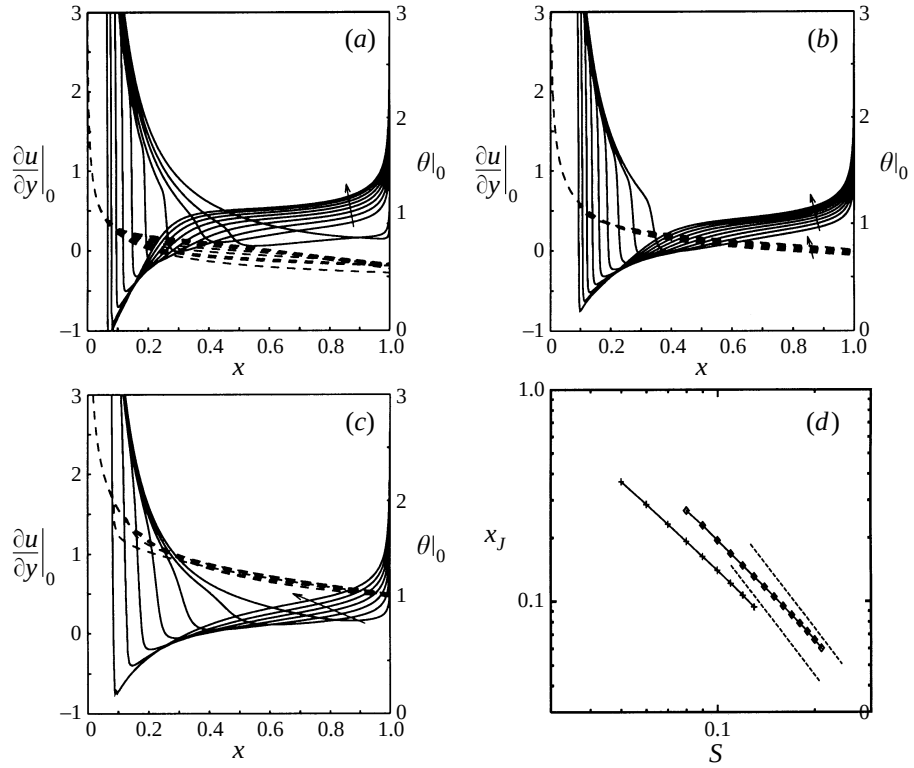

FIGURE 8. Skin friction (solid) and wall temperature (dashed) for (*a*) $Pr = 0.5$ and $S = 0.02$, 0.04, 0.06, 0.08, 0.1, 0.12, 0.14, 0.16, 0.18, 0.2; (*b*) $Pr = 1$ and $S = 0.05$, 0.06, 0.07, 0.08, 0.09, 0.1, 0.11, 0.12, 0.13; (*c*) $Pr = 3$ and $S = 0.02$, 0.04, 0.06, 0.08, 0.1, 0.12, 0.14. Values of S increasing as indicated by the arrows. Also plotted, in (*d*), is the position of the separation point as a function of S for $Pr = 0.5$ (lower curve) and 1. The dashed lines have slope -2.

previous Section, yield $u = O(S^{1/3})$ and $(y, \theta) = O(S^{-1/6})$. Essentially the same balance holds in the bulk of the bubble ($u_b^2/x_b \sim S\theta_b y_b/x_b \sim u_b/y_b^2$ and $u_b\theta_b y_b = O(1)$, with the subindex b denoting the properties of the bubble), and since compatibility of the solutions in the two regions requires $y_b = O(y)$ and $u_b = O(u)$, these estimations imply $\theta_b = O(\theta) = O(S^{-1/6})$ and $x_b = O(1)$, so the length of the bubble is of the same order as the length of the plate. Finally, the position of the separation point can be estimated from the condition that the momentum flux in the bubble, $O(u^2 y) = O(S^{1/2})$, must be of the order of the momentum flux in the wall jet at separation, $O(x_J^{-1/4})$, in order for the flow in the bubble to overcome the region of adverse pressure gradient. This condition yields $x_J = O(S^{-2})$, in agreement with the numerical results (see figure 8).

Local (tilde) variables analogous to those of §2.2 can be introduced to analyse the flow at the beginning of the bubble. Now, however, the temperature also needs be rescaled defining $\tilde{\theta} = x_J^{1/4}\theta$ and, with this new factor taken into account in equations (3) and (2), the rescaled pressure changes to $\tilde{p} = p/x_J^{1/2}$, and $\tilde{S} = Sx_J^{3/2}$. In addition, owing to the entrainment, the rescaled temperature of the separated jet is of order unity only for $\tilde{x} = O(1)$, but not beyond. The temperature of the recirculating fluid is much smaller ($\tilde{\theta} = O(\tilde{S}^{1/3})$ from the previous estimations), which introduces some changes in the asymptotic description of §2.2. First, the scaled temperature can still be written in the form (11), but $\tilde{\theta}_0(\tilde{y})$ must be extended as $\tilde{\theta}_0 = 0$ for $\tilde{y} < 0$

and $\Delta\tilde{\theta} = O(1)$ in the viscous sublayer of the interaction region for $(\tilde{x}/\tilde{S}^3) > 0$ to account for the small $\tilde{\theta}$ of the recirculating fluid. Second, immediately downstream of the interaction region, for $(\tilde{x}/\tilde{S}^3) \gg 1$ but $\tilde{x}$ still very small, $\Delta\tilde{\theta}$ is of order unity only in the shear layer of thickness $O\left[\tilde{S}(\tilde{x}/\tilde{S}^3)^{1/3}\right]$, and therefore the pressure changes by an amount of this order on crossing the shear layer but effectively suffers no further change across the recirculating fluid. As a consequence, the pressure on the viscous sublayer at the bottom of the recirculating flow is no longer of the order of the depth of the bubble, but of the order of the depth of the shear layer. Writing $\tilde{y}_b = O\left[\tilde{S}(\tilde{x}/\tilde{S}^3)^{m_1}\right]$ in this region, the entrainment of the shear layer leads to velocities of order $\tilde{S}^2(\tilde{x}/\tilde{S}^3)^{2/3}/\tilde{y}_b = O\left[\tilde{S}(\tilde{x}/\tilde{S}^3)^{2/3-m_1}\right] = O\left[\tilde{S}(\tilde{y}/\tilde{S})^{2/3m_1-1}\right]$ in the recirculating flow (see §2.4 and Gajjar & Smith 1983), while the balance of inertia, pressure and viscosity forces in the viscous sublayer (where $\tilde{y} = O(\tilde{y}_v)$, to be determined, and $\tilde{u} = O\left[\tilde{S}(\tilde{y}_v/\tilde{S})^{2/3m_1-1}\right]$) gives $m_1 = 10/21$ and $(\tilde{y}_v/\tilde{S}) = O(\tilde{x}/\tilde{S}^3)^{5/12}$.

The shear layer covers the whole of the separated jet when $\tilde{x} = O(1)$. For $\tilde{x} \gg 1$ the thickness of the jet grows as $\tilde{x}^{2/3}$, its velocity decays as $\tilde{x}^{-1/3}$, as well as its temperature (from the energy conservation condition), and the pressure variation across the jet, responsible for the pressure gradient on the viscous sublayer, is of order $\tilde{x}^{1/3}$. Writing $\tilde{y}_b = \alpha_1\tilde{x}^{n_1}$ for the depth of the bubble in this region, the usual order of magnitude analysis in the bubble and the viscous sublayer gives $\alpha_1 = O(\tilde{S}^{-3/7})$ and $n_1 = 5/21$, whereas the thickness of the viscous sublayer is of order $\tilde{x}^{5/12}/\tilde{S}^{1/4}$. This thickness becomes comparable to the depth of the bubble and to the thickness of the jet for $\tilde{x} = O(1/\tilde{S})$, corresponding to the bulk of the bubble, where the scaled velocity and temperature are both $O(\tilde{S}^{1/3})$.

It should be remarked that the structure just described involves a region of unstable stratification in the leading part of the bubble. This feature is confirmed by the numerical solutions of the boundary layer equations for the largest values of S reached, and it is not unlike the unstable stratification often reported near the corners of cavity flows (e.g. Ravi, Henkes & Hoogendoorn 1994). Though the stability of these steady solutions will not be analysed here, it seems reasonable to conjecture that the unstable stratification will play a role in the transient response and the transition to turbulence of these flows.

An analysis of the asymptotic limit $Pr \to \infty$ with $S_\infty = S/Pr^{2/3}$ finite can be carried out along the lines of §2.3. Equations (12)–(19) still hold, with the changes $\partial\theta/\partial y = 0$ at $y = 0$ and $\theta \to g_{1\infty}(\eta)/x^{1/4}$ for $x \to 0$, where $g_{1\infty}(\eta) = 3^{1/3}\exp(-\lambda\eta^3/24)/[4\lambda^{1/3}\Gamma(2/3)]$. Numerical solutions of this problem show features similar to those of §2.3, though the bubbles are somewhat smaller than in that case for the same values of S_∞. The skin friction and temperature of the wall in the region of the bubble are given in figure 9 for several values of S_∞.

Local (tilde) variables can be introduced once again to analyse the region of the bubble in the limit $S_\infty \to \infty$, with $\tilde{\theta} = x_J^{1/4}\theta$, $\tilde{p} = p/x_J^{1/2}$, $\tilde{S}_\infty = S_\infty x_J^{3/2}$, and the other scaled variables defined as in §2. In the small region around the separation point where $\bar{x} = \tilde{x}/\tilde{S}_\infty = O(1)$, the problem (20)–(26) is retrieved, with θ and g_∞ replaced by $\tilde{\theta}$ and $g_{1\infty}$. Now, however, the temperature of the fluid entering this region from the right must be taken as zero, to leading order, because the temperature of the recirculating fluid, $\tilde{\theta}_b$ say, is very small ($\tilde{\theta}_b = O(\tilde{S}_\infty^{1/3}) \ll 1$ in the bulk of the bubble; see below). In these conditions, the asymptotic form of the solution for $\bar{x} \gg 1$ consists of a constant-thickness streak of $\tilde{\theta} = O(1)$ over an effectively stagnant region whose depth grows linearly with $\bar{x}$. Putting $\tilde{y}_b = a\bar{x}$ into (27) and looking for a $\tilde{\psi}$ independent of $\bar{x}$, this equation can be integrated once to give $\partial^3\tilde{\psi}/\partial\tilde{Y}^3 = ag_{1\infty}[(2\tilde{\psi}/\lambda)^{1/2}]$, to be

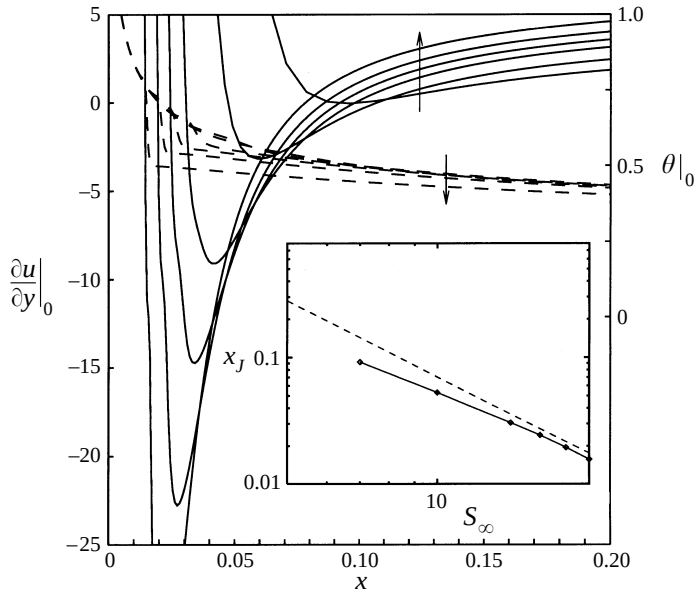

FIGURE 9. Skin friction (solid) and wall temperature (dashed) for $Pr \to \infty$ and $S_\infty = 7$, 10, 14, 16, 18 and 20, increasing as indicated by the arrows. Inset: separation point as a function of S_∞. The dashed line has slope −2.

solved with the conditions $\tilde{\psi}(0) = \tilde{\psi}'(0) = \tilde{\psi}''(0) = 0$ and $\tilde{\psi}''(\infty) = \lambda$. The solution of this problem, which holds for any $\bar{x} > 0$, determines $a \approx 0.0688$ and the stream function in the separated streak. This result can be used as initial condition for equation (27) at $\bar{x} = 0$, and (27) can then be solved for $\bar{x} < 0$, with the boundary conditions $\tilde{\psi} = \partial\tilde{\psi}/\partial\tilde{Y} = 0$ at $\tilde{Y} = 0$ and $\partial^2\tilde{\psi}/\partial\tilde{Y}^2 - \lambda = \partial^3\tilde{\psi}/\partial\tilde{Y}^3 = 0$ for $\tilde{Y} \to \infty$. The resulting skin friction is included in figure 7 (dashed curve).

The pressure variation across the fluid below the streak is of order $\tilde{\theta}_b\tilde{y}_b$. It becomes of order unity when $\tilde{x} = O(\tilde{S}_\infty^{2/3})$ (where use has been made of the result $\tilde{\theta}_b = O(\tilde{S}_\infty^{1/3})$ mentioned before, and $\tilde{y}_b = O(\tilde{x}/\tilde{S}_\infty)$), and dominates over the pressure variation in the streak when $\tilde{x} \gg \tilde{S}_\infty^{2/3}$. Writing $\tilde{y}_b = \alpha_{1\infty}(\tilde{x}/\tilde{S}_\infty)^{n_{1\infty}}$ in this latter region, the vertical hydrostatic balance and the momentum equation can be integrated to give $\tilde{p} = \tilde{\theta}_b(\tilde{y}_b - \tilde{y})$ and $\tilde{u} = (\mathrm{d}\tilde{y}_b/\mathrm{d}\tilde{x})\tilde{S}_\infty\tilde{\theta}_b\tilde{y}(3\tilde{y}_b - 2\tilde{y})/6$, whereas the condition that the outer shear should matter ($\partial\tilde{u}/\partial\tilde{y}|_{\tilde{y}_b} = \lambda$ for $\tilde{x} \ll 1$) determines $n_{1\infty} = 1/2$ and $\alpha_{1\infty} = \left(3\lambda/\tilde{\theta}_b\right)^{-1/2}$, and implies that the bubble cannot extend to very large values of $\tilde{x}$, as in §2.3. On the other hand, the thickness $\tilde{\delta}_T$ of the streak on top of the bubble decreases as $\tilde{u}$ increases, until heat conduction comes into play in the streak when $\tilde{x} = O(\tilde{\theta}_b\tilde{S}_\infty)^{1/3}$. For still larger values of $\tilde{x}$ the streak grows on both sides of the dividing streamline and its thickness $\tilde{\delta}_T$ is determined by the convection–conduction balance $\tilde{u}/\tilde{x} \sim 1/\tilde{\delta}_T^2$, giving $\tilde{\delta}_T = O\left[\tilde{x}^{3/4}/(\tilde{\theta}_b\tilde{S}_\infty)^{1/4}\right]$, while the condition of energy conservation ($\tilde{u}\tilde{\theta}\tilde{\delta}_T$ of order unity) implies $\tilde{\theta} = O\left[(\tilde{\theta}_b\tilde{S}_\infty\tilde{x})^{-1/2}\right]$. Part of the fluid in the streak recirculates on reaching the end of the bubble, at some $\tilde{x} = O(1)$, and therefore the temperature $\tilde{\theta}_b$ of the fluid in the bubble is of the order of the temperature of the streak there, which justifies the result $\tilde{\theta}_b = O(\tilde{S}_\infty^{1/3})$ given before. Notice, however, that the heat conduction is negligible in the scale of the depth of the bubble, of order $\tilde{S}_\infty^{-2/3}$. Finally, since the depth of the thermal layer beyond the bubble is $y = O(S_\infty^{-1/6})$

(a result obtained as when Pr is not large), consistency with the previous estimation of the depth of the bubble requires $x_J = O(S_\infty^{-2})$.

In the opposite limit of small Prandtl numbers, the natural-convection boundary layer tends to become thicker than the jet. The numerical results show that the bubble shortens with increasing Pr, and analysis suggests that a number of distinguished limits could exist depending on the relation between the parameters Pr and S. If Pr is smaller than any power of S, the thermal layer tends to that corresponding to a point release of a finite (negative) heat flux at $x = 0$. In this limit the thickness of the thermal layer decreases monotonically toward the edge of the plate, leading to no adverse gradient on the jet and no separation, in line with the tendency shown by the numerical results.

4. Summary and further comments

The boundary layer problem for mixed convection in a wall jet over a finite-length horizontal cold or insulating plate has been formulated and numerically solved taking into account the upstream information propagation due to the buoyancy-induced pressure.

In the asymptotic limit of very small Froude numbers separation occurs in a Bowles–Smith interaction region near the origin of the jet, followed by a recirculation bubble that extends over a sizeable fraction of the plate and a region of buoyancy-dominated flow further downstream. The scales of the different regions appearing in the asymptotic solution have been determined by order of magnitude analyses.

For large values of the Prandtl number the opposing pressure gradient is confined to a thin thermal layer at the base of the jet. Separation of this layer in the limit of small Froude numbers occurs in a short conduction-free region where the governing equations are parabolic in the upstream direction, and is followed by a short recirculation bubble. The buoyancy-induced pressure gradient rapidly becomes favourable and dominates the flow over the rest of the plate.

In the distinguished limit $S_0 = S/Pr^{1/2} = O(1)$, $Pr \to 0$ the thermal layer is much thicker than the wall jet and imposes a pressure distribution on it that may lead to separation, but the jet does not affect the thermal layer. The structure of the interaction region around the separation point when $S_0 \to \infty$ is as for $Pr = O(1)$, but the flow in the bubble has a different structure somewhat downstream of the interaction region.

Separation of a cold jet over an insulated plate may lead to a small region of unstable stratification in the fore part of the bubble, because energy conservation requires that the temperature defect of the separated jet decrease as the jet progresses from the separation point, implying that the temperature defect is smaller when the fluid recirculates from the rear part of the bubble than it was at separation. The asymptotic solution for $S \to \infty$ is slightly different from the one for a cold plate.

The flow over an insulated plate may be relevant to the much studied problem of thermally driven cavities, where the fluid filling a rectangular container is set in motion by the action of a temperature difference established between its vertical walls, the horizontal walls being insulated. For large Rayleigh numbers two boundary layers appear on the vertical walls, which turn around the lower cold and upper hot corners of the cavity and emerge as wall jets on the horizontal walls. In some conditions a rapid divergence of these jets is observed not far from their origins, involving separation from the horizontal walls and recirculation regions between the jets and the vertical walls. The importance of such phenomena to the overall flow

was pointed out by Janssen & Henkes (1995), who found that the Kelvin–Helmholtz instability of the separated jets is one of the causes of transition to turbulence in these flows. Ivey (1984) and Paolucci & Chenoweth (1989) interpreted the divergence of the wall jets as internal hydraulics jumps and worked out qualitative criteria for the first appearance of the jumps and the bifurcation of the flow to a non-steady state in terms of the classic theory of hydraulic jumps (Turner 1973). Patterson & Armfield (1990) and Ravi *et al.* (1994), among others, criticized the lack of definiteness of the hydraulic jump characteristics and attributed the separation and recirculation regions to the existence of plumes in the locally unstable stratification prevailing near the corners. It may be appropriate to note here that while a characterization of the laminar hydraulic jumps probably cannot be very precise in the framework of the classic theory, the flow near the separation points bears a striking resemblance to the ones described in this paper. The resemblance disappears further downstream (the jets in a driven cavity need not even reattach), but this may be an effect of the downstream boundary conditions used here, which have no correspondence with the driven cavity configuration.

Discussions with Dr R. Bowles on many aspects of this work are gratefully acknowledged. The work was partially supported by the DGICYT under grants PB95-0008 and PB94-0400.

REFERENCES

Bowles, R. I. & Smith, F. T. 1992 The standing hydraulic jump: theory, computations and comparisons with experiments. *J. Fluid Mech.* **242**, 145–168.

Daniels, P. G. 1992 A singularity in thermal boundary-layer flow on a horizontal surface. *J. Fluid Mech.* **242**, 419–440.

Daniels, P. G. 1993 High Rayleigh number thermal convection in a shallow laterally heated cavity. *Proc. R. Soc. Lond.* A **440**, 273.

Daniels, P. G. & Gargaro, R. J. 1993 Buoyancy effects in stably stratified horizontal boundary-layer flow. *J. Fluid Mech.* **250**, 233–251.

Gajjar, J. S. B. & Smith, F. T. 1983 On hypersonic self-induced separation, hydraulic jumps and boundary layers with algebraic growth. *Mathematika* **30**, 77–91.

Glauert, M. B. 1956 The wall jet. *J. Fluid Mech.* **1**, 625–643.

Higuera, F. J. 1993 Natural convection below a downward facing horizontal plate. *Eur. J. Mech.* B **12**, 289–311.

Higuera, F. J. 1994 The hydraulic jump in a viscous laminar flow. *J. Fluid Mech.* **274**, 69–92.

Ivey, G. N. 1984 Experiments on transient natural convection in a cavity. *J. Fluid Mech.* **144**, 389–401.

Janssen, R. J. A. & Henkes, R. A. W. M. 1995 Influence of Prandtl number on instability mechanisms and transition in a differentially heated square cavity. *J. Fluid Mech.* **290**, 319–344.

Paolucci, S. & Chenoweth, D. R. 1989 Transition to chaos in a differentially heated vertical cavity. *J. Fluid Mech.* **201**, 379–410.

Patterson, J. C. & Armfield, S. W. 1990 Transient features of natural convection in a cavity. *J. Fluid Mech.* **219**, 469–497.

Ravi, M. R., Henkes, R. A. W. M. & Hoogendoorn, C. J. 1994 On the high-Rayleigh-number structure of steady laminar natural-convection flow in a square enclosure. *J. Fluid Mech.* **262**, 325–351.

Smith, F. T. 1982 On the high Reynolds number theory of laminar flows. *IMA J. Appl. Maths* **28**, 207–281.

Smith, F. T. & Duck, P. W. 1977 Separation of jets or thermal boundary layers from a wall. *Q. J. Mech. Appl. Maths* **30**, 143–156.

SCHNEIDER, W. 1979 A similarity solution for combined forced and free convection flow over a horizontal plate. *Intl J. Heat Mass Transfer* **22**, 1401–1406.

SCHNEIDER, W., STEINRÜCK, H. & ANDRE, G. 1994 The breakdown of boundary layer computations in case of the flow over a cooled flat plate. *Z. Angew. Math. Mech.* **74**, T402–T404.

STEINRÜCK, H. 1994 Mixed convection over a cooled horizontal plate: non-uniqueness and numerical instabilities of the boundary-layer equations. *J. Fluid Mech.* **278**, 251–265.

TURNER, J. S. 1973 *Buoyancy Effects in Fluids*. Cambridge University Press.